Pharmacokinetics of intravenously injected Tc-99m labeled ferrite nanobeads

Chao-Ming Fu,[1,a)] Yuh-Feng Wang,[2,3] Yu-Feng Guo,[1] Li-Shin Wang,[1] May-Haw Chuang,[3] and Thau-Ming Cham[3]
[1]*Department of Physics, National Taiwan University, Taipei 10617, Taiwan*
[2]*Department of Nuclear Medicine, Buddhism Dalin TzuChi General Hospital, Chia-Yi 62247, Taiwan*
[3]*Faculty of Pharmacy, Kaohsiung Medical University, Kaohsiung 80708, Taiwan*

(Presented 12 November 2008; received 2 October 2008; accepted 7 December 2008; published online 16 March 2009)

We study the time varying biodistribution of ferrite (Fe_3O_4) nanoparticles upon *in vivo* injection. For this purpose, a novel process of directly labeling radioactive Tc-99m with ferrite nanoparticles was developed. The radiobeads serve as a tracer to provide information on the uptake of injected particles by organs. In the course of our study, Tc-99m labeled ferrite beads were intravenously injected into the tail vein of rats. The time course of changes in the radio-intensity of heart, lung, and liver could be achieved by real-time scintigraphic images. It was observed that the particle uptake by organs is very fast and completed within the first few minutes after intravenous injection. The pharmacokinetic behavior of the radiobead uptake was quantitatively described by a two-compartment model. © *2009 American Institute of Physics*. [DOI: 10.1063/1.3074131]

I. INTRODUCTION

Biocompatible iron oxide magnetic nanoparticles (MNPs) can be used in a wide variety of biomedical applications.[1–10] Magnetic separation is one of the practices that utilize the MNPs to label biological entities, such as DNA, proteins, and cells, for purification and enrichment. The magnetically labeled bioentities can then be advanced for magnetic detection in a lab-on-a-chip approach utilizing a giant magnetoresistance detector[10] or magnetoimpedance sensing, etc.[11,12]

Another practical application is the use of MNPs as contrast agents for *in vivo* diagnosis in magnetic resonance imaging (MRI).[13] It has been demonstrated that the iron oxide MNPs notably enhance the image contrast and efficiently differentiate healthy and pathological tissues. The iron oxide nanoparticles, due to their low toxicity, have received U.S. Food and Drug Administration approval to be used as MRI signal enhancers. Progressive development has been done by using human-grade superparamagnetic iron oxide MNPs for magnetic resonance-based tracking of intravenously injected magnetically labeled stem cell and for monitoring of the distribution of transplanted stem cells in the body.[13]

The MNPs have shown great therapeutic promise in utilization as a carrier to be conjugated with chemotherapeutic drugs and to target disease sites by external magnetic fields.[14] The magnetic control of cytotoxic drug release in cancer treatment takes the advantage of a highly localized drug concentration and diminishing side effects. This principle is also explored in radiotherapy, which utilizes MNPs labeled with radio-nuclides in order to enrich radioactivity at the desired location and consequently reduce damage to surrounding tissue.[9] To realize practical clinical applications, the knowledge of organ distribution and the final fate of the injected drug/carrier complex is necessary.

In our previous works,[15,16] we have developed a novel approach to directly label the radioisotope technetium-99m (Tc-99m) with ferrite nanoparticles. The approach needs no chemical coating overlayer on the ferrite nanoparticles and therefore keeps the particle size small. As prepared, radiolabeled ferrite nanoparticles have shown high labeling efficiency for the half-life period of Tc-99m and are, accordingly, applicable to long term monitoring of the organ uptake of injected nanoparticles. Since the time resolution of dynamic scintigraphic images, detected by a gamma camera, can achieve several frames per second, the methodology is also able to investigate the initial stage time varying uptake and release of particles by the organ under study upon intravenous injection. In this article, we present the *in vivo* study of the pharmacokinetic behavior of intravenously injected ferrite nanoparticles labeled with Tc-99m, and we explore the initial stage uptake and translocation of nanoparticles by heart, lung, and liver.

II. EXPERIMENTS

The ferrite (Fe_3O_4) nanoparticles used in this study were synthesized from a reaction solution of $FeCl_2$ (0.05*M*) and $FeCl_3$ (0.05*M*) and an adjusting solution of NH_4OH (50 ml). The synthesis was done at room temperature, and the *p*H value of the aqueous solution was near neutral.[17] At the final stage, the black nanoparticles of Fe_3O_4 were precipitated in the solution. X-ray diffraction characterization has shown a pattern typical of Fe_3O_4. The average diameter of a particle is around 10–25 nm, as deduced from an analysis of the x-ray diffraction peak by Langevin's formula. The dried powder of as prepared particles shows a nearly superpara-

[a)]Author to whom correspondence should be addressed. Electronic mail: chaomingfu@phys.ntu.edu.tw.

magnetic behavior characterized by vibrating sample measurements. For details the reader is referred to Refs. 15 and 16.

The radiotracer, Tc-99m with a radioactivity of 1.11 GBq (30 mCi), was prepared as routine process in nuclear medicine at a hospital facility. To label the ferrite nanoparticles with a radiotracer, the preprocessed Tc-99m was injected into a sterile vacuum collecting vial (5 ml in volume). Subsequently, a stannous solution (0.5 ml) served as a reducing agent, which reduced the surface charge of Tc-99m to a suitable condition for labeling. It was injected into the vial and stirred for 10 s. In the meanwhile, a diluted ferrite nanoparticle solution was prepared by extracting 0.1 ml solution containing the ferrite nanoparticles and diluting it with 0.9 ml pyrogen-free isotonic saline. Then, the diluted ferrite nanoparticle solution of 0.5 ml was added into the vial containing the Tc-99m. The resultant solution was kept at room temperature for 2 min in order to achieve an entire labeling of the radiotracer with ferrite nanoparticles.

The labeling efficiency of as prepared radiobeads was checked by an instant thin-layer chromatography method before each *in vivo* experiment. The radio-labeling efficiency was more than 90% initially and reduced to less than 5% within the first 50 min. The labeling efficiency was nearly unvarying in the half-life time of Tc99m.

III. RESULTS AND DISCUSSION

To explore the time evolution of *in vivo* biodistribution of nanobeads, the Tc-99m labeled ferrite nanoparticles were intravenously injected into the tail vein of Wistar rats (male, 200–250 g). The scintigraphic images were monitored by a planar type gamma camera (GE, DST XLi) with a parallel collimator. The radio-intensity of each organ was analyzed by a graphic tool from a selected area of the scintigraphic images and was normalized by that of the whole rat body. The scintigraphic images, obtained from the planar gamma camera, have been autorescaled to the brightest intensity of each scintigram by the equipment software. Thus, the radio-intensity in a scintigraphic image is a relative result rather than an absolute value. In the course of this study, we have further normalized the radio-intensity by that of the whole body.

Figure 1 demonstrates the time evolution of the normalized radio-intensity of the upper chest (attributed mainly to lung and heart uptake) and lower chest (mainly due to liver uptake) of a rat upon an *in vivo* (i.v.) injection of 12 nm ferrite particles labeled as Tc-99m radioisotope. As shown in Fig. 1, the normalized radio-intensity of the upper chest increases rapidly, in approximately logarithmical function of time, upon the administration of intravenously injected ferrite radiobeads. After reaching a maximum, the radio-intensity decreases in a slow slope as a function of time. On the other hand, the radio-intensity of the lower chest increases monotonically to a plateau after about 60 s. The radio-intensity of this plateau is far apart from the upper chest value after a long duration. Since the normalized radio-intensity is related to the ratio of radiobead uptake by organs to that by the whole body, the observed time evolution of the

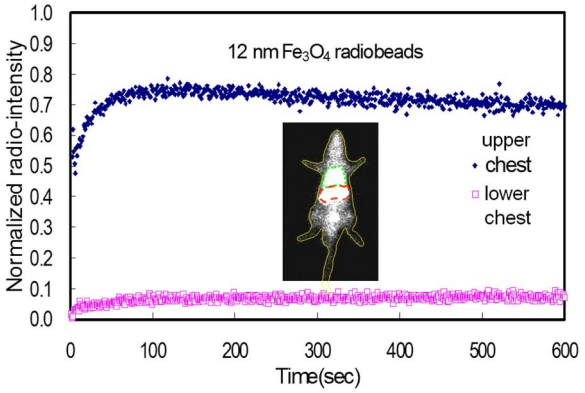

FIG. 1. (Color online) The time evolution of biodistribution in a rat upon i.v. injection of ferrite radiobeads. The inset shows the scintigram. The brightness represents radio-intensity of radiobead uptake.

radio-intensity is ascribed to the kinetic process of absorption and excretion of radiobeads by the organism.

Further, an analysis was carried out in order to tell apart the kinetic behavior of radiobead uptake by lung, heart, and liver. In the course of this analysis, the radio-intensity of a selected area was divided by the selected area and further normalized to that of the whole body, divided by the area of the whole body. We call this value the normalized radio-density. Figure 2 displays the initial stage time variation of the normalized radio-density of lung, heart, and liver of rat upon i.v. injection of 12 nm ferrite radiobeads. As illustrated in Fig. 2, there appear several characteristic features. (1) A characteristic feature of the heart is that the normalized radio-density rises rapidly within the first few seconds to a peak value, and after the peak the radio-intensity decreases slowly as a function of time. (2) A characteristic feature of the lung is that the normalized radio-density increases with increasing time, in approximately a logarithmical function. (3) A characteristic feature of the liver is that the normalized radio-density increases nonlinearly toward a low plateau. (4) Each of the normalized radio-density values for heart and lung approaches toward a common plateau after about 60 s, and the value of this plateau is far apart from that of the liver after a long duration. The observed time variation of the

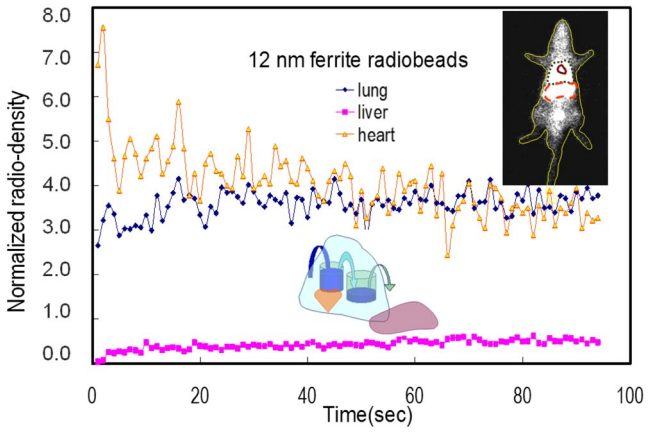

FIG. 2. (Color online) The time varying biodistribution in heart, lung, and liver upon i.v. injection of the ferrite radiobeads. The insets display the scintigram and the two-compartment model represented by perfusion and relocation of injected beads.

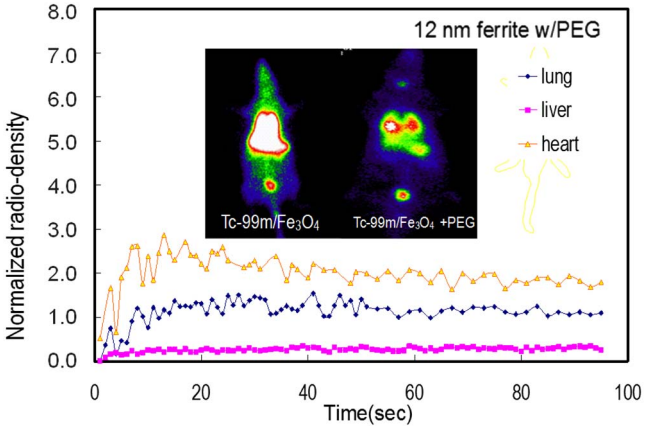

FIG. 3. (Color online) The initial stage time evolution of biodistribution in a rat upon i.v. injection of ferrite radiobeads conjugated with PEG.

normalized radio-density of each organ is in correspondence to the pharmacokinetics of radiobead uptake by the organs.

The compartmental model has been well used to describe the pharmacokinetic process of absorption and excretion of substances upon administration.[18] To qualitatively describe the observed initial stage characteristic of the radiobead uptake, we have attempted to adapt a two-compartment model where one compartment represents the heart and the other the lung. The variation in radiobead concentration in the heart and lung is in accordance with the cardiac diastole and systole processes for perfusion and ejection of radiobeads in each organ. At the initial stage (from time zero) upon i.v. injection, the intravenous radiobead stream fills into the heart. After early rapid filling, the radiobead stream perfuses into the lung under an ejection process of ventricular systole. During the cardiac cycles, the radiobead flow was sequentially driven from the lung into the liver and then increased slowly toward a nearly constant retaining value in the long run.

The retaining concentration of radiobeads in organs strongly depends on the properties of beads, such as particle size and surface charge. As reported, the uptake of radiobeads is associated with the mononuclear phagocytic system (MPS).[16] To diminish the uptake by MPS, a surface modification of coating poly(ethyelene glycol) (PEG) onto the particles is used to reduce the surface charge effect.[19] For comparison we have performed a study of the biodistribution of ferrite radiobeads conjugated with PEG. As shown in Fig. 3, the normalized radio-density of the uptake by heart increases rapidly in the first 10 s and sequentially decreases in an approximately inverse exponential function of time. The specifics of the initial uptake are obviously different from those of ferrite beads without the PEG overlayer.

This result is in accord with the appearance of the scintigraphic images. The right insets in Fig. 3 display the scintigraphic images taken at 5 min after intravenous injection of radiobeads with PEG overlayer. For radiobeads conjugated with PEG, most of the injected beads escape from the uptake by liver and reach a nearly even concentration in the body. On the other hand, most of the injected radiobeads without the PEG modification are taken up by the liver and lung. This result manifests the alteration of the pharmacokinetic behavior by surface charge modification with PEG.

In conclusion, a novel process is developed to prepare directly labeled Tc-99m ferrite beads, which serve as a tracer to monitor the time varying particle uptake by organs. The pharmacokinetic behavior of intravenously injected radiobeads is ascribed to the absorption and excretion process of particles among the heart, lung, and liver and can be qualitatively described by a two-compartmental model. The characteristic features of particle uptake by organs can be altered by PEG modification of the particles. Further analysis of the quantitative parameters of nanoparticle pharmacokinetics is of interest to biomedical applications.

ACKNOWLEDGMENTS

This work was supported by National Science Council, Taiwan under Grant No. NSC 95-2112-M-002-055-MY3.

[1] S. Sieben, C. Bergemann, A. Lübbe, B. Brockmann, and D. Rescheleit, J. Magn. Magn. Mater. **225**, 175 (2001).
[2] Y. Haik, V. Pai, and C.-J. Chen, J. Magn. Magn. Mater. **194**, 254 (1999).
[3] R. Weissleder, A. Bogdanov, E. A. Neuwelt, and M. Papisov, Adv. Drug Delivery Rev. **16**, 321 (1995).
[4] A. Jordan, P. Wust, R. Scholz, U. O. Häfeli, W. Schutt, J. Teller, and M. Zborowski, *Scientific and Clinical Applications of Magnetic Carriers* (Plenum, New York, 1997), p. 569.
[5] M. Ogiue-Ikeda, Y. Sado, and S. Ueno, IEEE Trans. Magn. **40**, 3018 (2004).
[6] K. Nishimura, M. Hasegawa, Y. Ogura, T. Nishi, K. Kataoka, and H. Handa, J. Appl. Phys. **91**, 8555 (2002).
[7] A. S. Lubbe, C. Bergemann, W. Huhnt, T. Fricke, H. Riess, J. W. Brock, and D. Huhn, Cancer Res. **56**, 4694 (1996).
[8] U. O. Häfeli, S. M. Sweeney, B. A. Beresford, E. H. Sim, and R. M. Macklis, J. Biomed. Mater. Res. **28**, 901 (1994).
[9] U. O. Häfeli, S. M. Sweeney, B. A. Beresford, B. A. Humm, and R. M. Macklis, Nucl. Med. Biol. **22**, 147 (1995).
[10] D. L. Graham, H. A. Ferreira, and P. P. Freitas, Trends Biotechnol. **22**, 455 (2004).
[11] L. Xu, H. Yu, M. S. Akhras, S. J. Han, S. Osterfeld, R. L. White, N. Pourmand, and S. X. Wang, Biosens. Bioelectron. **24**, 99 (2008).
[12] G. V. Kurlyandskaya, V. Fal Miyar, A. Saad, E. Asua, and J. Rodriguez, J. Appl. Phys. **101**, 054505 (2007).
[13] L. S. Politi, M. Bacigaluppi, E. Brambilla, M. Cadioli, A. Falini, G. Comi, G. Scotti, G. Martino, and S. Pluchino, Stem Cells **25**, 2583 (2007).
[14] Q. A. Pankhurst, J. Connolly, S. K. Jones, and J. Dobson, J. Phys. D: Appl. Phys. **36**, R167 (2003).
[15] C. M. Fu, Y. F. Wang, Y. C. Chao, H. S. Huang, and M. D. Yang, IEEE Trans. Magn., **40**, 3001 (2004).
[16] C. M. Fu, Y. F. Wang, Y. F. Guo, T. Y. Lin, and J. S. Chiu, IEEE Trans. Magn., **41**, 4120 (2005).
[17] M. Abe and Y. Tamaura, Jpn. J. Appl. Phys., Part 2 **22**, L511 (1983).
[18] S. J. Kovacs, B. Barzilai, and J. E. Perez, Am. J. Physiol. Heart Circ. Physiol. **252**, 178 (1987).
[19] R. Gref, *Synthesis, Functionalization and Surface Treatment of Nanoparticles* (American Scientific, Stevenson Ranch, CA, 2003), p. 233.